Aristovich, K. Y. & Khan, S. (2010). Automatic procedure for realistic 3D finite element modelling of human brain for bioelectromagnetic computations. Journal of Physics: Conference Series, 238(1), 012065. doi: 10.1088/1742-6596/238/1/012065

CITY UNIVERSITY LONDON
EST 1894

City Research Online

Original citation: Aristovich, K. Y. & Khan, S. (2010). Automatic procedure for realistic 3D finite element modelling of human brain for bioelectromagnetic computations. Journal of Physics: Conference Series, 238(1), 012065. doi: 10.1088/1742-6596/238/1/012065

Permanent City Research Online URL: http://openaccess.city.ac.uk/14368/

Automatic procedure for realistic 3D finite element modelling of human brain for bioelectromagnetic computations

K Y Aristovich and S H Khan

School of Engineering and Mathematical Sciences, City University London, Northampton Square, London EC1V 0HB, UK

E-mail: kirill.aristovich.1@city.ac.uk

Abstract. Realistic computer modelling of biological objects requires building of very accurate and realistic computer models based on geometric and material data, type, and accuracy of numerical analyses. This paper presents some of the automatic tools and algorithms that were used to build accurate and realistic 3D finite element (FE) model of whole-brain. These models were used to solve the forward problem in magnetic field tomography (MFT) based on Magnetoencephalography (MEG). The forward problem involves modelling and computation of magnetic fields produced by human brain during cognitive processing. The geometric parameters of the model were obtained from accurate Magnetic Resonance Imaging (MRI) data and the material properties – from those obtained from Diffusion Tensor MRI (DTMRI). The 3D FE models of the brain built using this approach has been shown to be very accurate in terms of both geometric and material properties. The model is stored on the computer in Computer-Aided Parametrical Design (CAD) format. This allows the model to be used in a wide a range of methods of analysis, such as finite element method (FEM), Boundary Element Method (BEM), Monte-Carlo Simulations, etc. The generic model building approach presented here could be used for accurate and realistic modelling of human brain and many other biological objects.

1. Introduction

The problem of accurate modelling of biological objects is a well established research area and it has been widely discussed in recent literature. The problem is more relevant to cases when modelling of human body organs, such as heart, bones, or even brain behaviour is needed with or without the presence of any external excitations.

Modern simulation methods in biomedical areas are becoming increasingly efficient due to the availability of powerful and relatively cheap desktop computing resources. However, some biological problems require very accurate computer models which must be built in order to perform computer simulations. Computer models must be as close to the real object as possible in order to satisfy required accuracy. This plays a key role in all sorts of analysis, but especially in those where excitation sources are much smaller than the biological object (for example, neuronal effects inside the brain, or microsurgery of the eye).

In biomedical modelling it is also essential to get realistic models for a particular subject noninvasively. Even small differences in structure can lead to a large errors in analyses, and therefore to incorrect conclusions. The well-known imaging modalities, such as MRI (Magnetic Resonance Imaging), CT (Computerized Tomography), or SPECT (Single Positron Emission Computer Tomography) can be used as for physical data needed for building numerical computer models.

Existing techniques being discovered in literature however cannot satisfy required accuracy, especially in the field of brain tomography. None of the existing reconstruction methods can reach the theoretical resolution of MRI.

The aim of the work presented here is to highlight the automatic procedure used for biological object reconstruction being developed for high-resolution brain model development. The main advantage of the procedure is that it reaches the theoretical limitations of MRI, and at the same time obtained model is flexible in terms of computational method and resources as it is stored in parametrical computer-aided format (CAD) and could be easily converted into any known modelling formats.

Human brain model, developed at City University London using the procedure presented in the paper is believed to be the most accurate in terms of geometry and material properties compared to existing models.

2. Accurate geometrical reconstruction

Accurate geometrical reconstruction is dictated by the mathematical solution, especially in 3D problems, solved by computer simulations. There are two ways of geometrical description of the model – parametric and triangular. First approach operates with the 3D parametric spline curves, surfaces and volumes which approximates required real object. It is also known as the Solid Modelling (SM) approach Second method operates with the points, straight lines, and triangular surfaces. It is also called the Direct Mesh Generation (DMG) method.

With using DMG it is not possible to change the model during the solution without recreating full model from the very beginning. Parametric approach is much more preferable as the model, reconstructed in this form, is more accurate, contains more information about the object, and could be easily used in any field of analysis. Note that the triangularization also could be performed on the parametric model with required parameters and it is much faster than direct triangularization method.

In case of biological modelling one of the most important properties of the mathematical model is the ability of optimization. The SM scheme, in opposite to DMG, allows optimization which is shown in Figure 1. Presented diagram shows particularly how SM approach is working in case of finite element modelling (FEM). Developed automatic geometrical SM procedure could be described as direct combination of following steps where the primary input to the procedure is the MRI scan, and output is the parametric geometrical solid model of the object. All figures are related to the human brain model for the particular subject, aged 21, male. High-quality 1mm resolution images were taken with the distance between slices of 2mm. Overall number of images in the scan is 150.
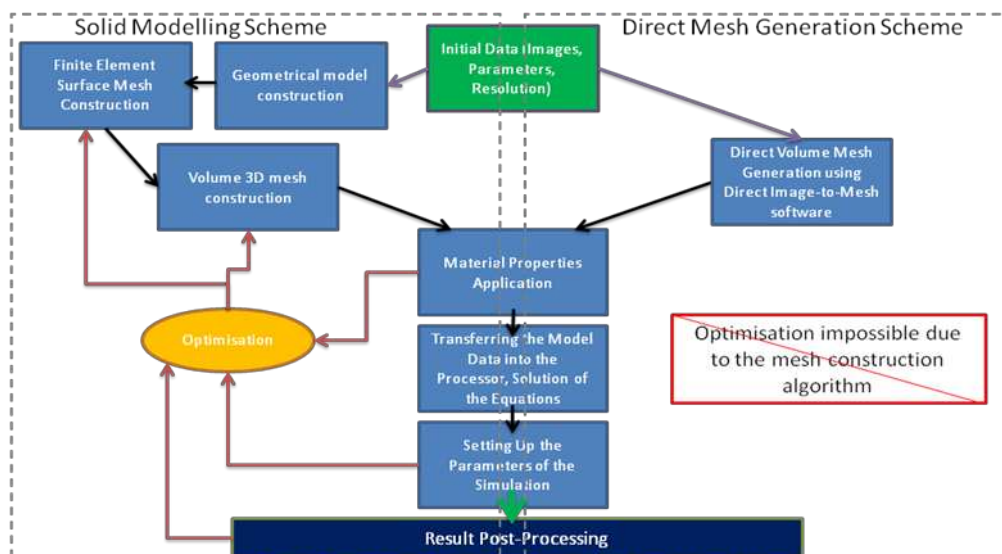
Figure 1. Solid Modelling (SM) and Direct Mesh Generation (DMG) schemes.

*2.1. Grey/white matter division and 2D edge reconstruction*

The first actual filtering step is the white/grey mated splitting from MRI image. This division plays significant role as it is the only geometrically structured part of the human brain and it could be easily detected. The detection algorithm is based on the combination of existing edge detection algorithms [3-4] and Region Growing algorithm [4-5]. It was performed in the MIPAV [2] software. Then the edges of white and grey matter is detected automatically and stored in the file as parametrical spline curves in 2D. The result of first two steps could be observed in Figure 2. Procedure repeats for each MRI slice. So the outcome of this step is 150 files with stored parametric edges for both white and grey matter. Note that the internal edges of grey matter are at the same time external edges of white matter, so the final step contains comparison and appropriate correction of the white matter boundaries.

2.2. Geometrical parameterization and closure

Each of the 2D parametric curve then transformed into 3D space by stacking respective slices one on top of each other with the 2mm distance between them according to the resolution step of MRI. Brain surface is very complex from the general point of view, but at the same time it is not self-intersecting, and therefore, the external edges are. This means the edges of the white and grey matter should be organized as closed contours. So the closure Geometrical Closure Algorithm (GCA) [6] is performed together with the self-intersection automatic checking in order to close the open contours and avoid self-intersection. 3D spline curves combined together is shown in Figure 3.
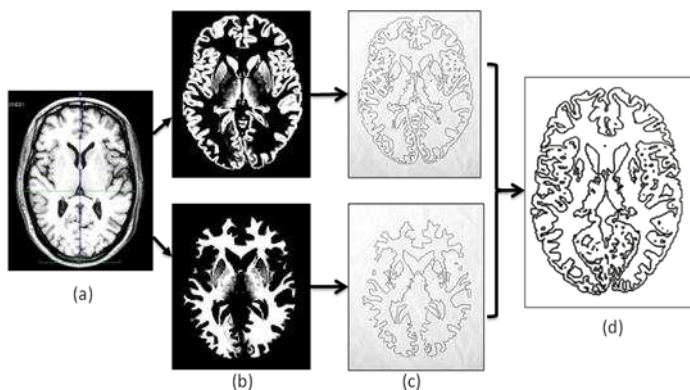
Figure 2. Grey/white matter division and 2D edge reconstruction. (a) Filtered single MRI slice, (b) white (bottom) /grey (top) matter filter, (c) 2d edge reconstruction for white and grey matter, and (d) final parametric edges approximated by spline curves.
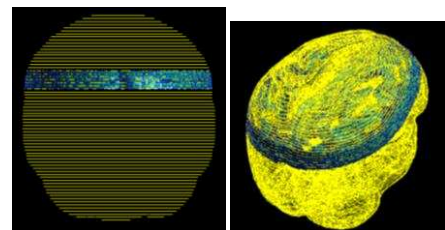
Figure 3. Parametrical spline curves representing geometrical boundaries of the brain, isometric view (left), and perpendicular to the slice surface view (right).

2.3. 3D parametrical surface lofting

The most significantly developed part of the geometrical reconstruction is the special Surface Lofting Algorithm. This algorithms allows automatically generate and connect external surfaces of the white and grey matter of the human brain from previously discussed combination of 3D parametrical curves representing the edges of each slice. General surface lofting procedure is well-known, commonly used in CAD software and could be observed in [7]. Briefly it is the method of surface creation which based on two curves. The network of perpendicular to the main spline curves is created with the specified

boundary conditions. This network then becomes a NURBS (Non-uniform rational B-spline) surface in 3D. Our approach is based on this method with the specific modifications discussed below.

Each 2D slice contains the boundary of the reconstructed object; therefore in two neighbor slices the surface connecting boundaries of one slice with the boundaries of another slice should be created. The example of this lofting procedure could be observed in Figure 4. Let us assume 3 slices stacked together with one curve on each slice. Let n will be the number of the middle slice, so C_{n-1}, C_n, and C_{n+1} are the curves of (n-1)-th, n-th, and (n+1)-th slice respectively. Also assume that the NURBS surface between C_{n-1} and C_n is already created (blue). The NURBS mesh for this surface contains curves $<D^1_{n-1}, \ldots, D^4_{n-1}>$. This curves intersecting with the main curve C_n give the points of intersection (base points) $<P^1_n, \ldots, P^4_n>$. Procedure starts with the points of intersection evaluation for curve C_{n+1}. The number of the points in general case is chosen to be exactly the same as for the previous main curve C_n. The position of each point P^m_{n+1} is found by the minimal distance from the point P^m_n to the curve C_{n+1}:

$$P^m_{n+1}: \quad \|P^m_{n+1}, P^m_n\| = \min\|P^m_n, C_{n+1}\| \tag{1}$$

where $\|\ \ \|$ is the distance operator. After all points have been evaluated the NURBS curve D^m_n is created between each corresponding point by the rule of tangential equivalence with the previous NURBS surface:

$$D^m_n = D^m_n\{ P^m_n; P^m_{n+1} \mid t[D^m_n, P^m_n] = t[D^m_{n-1}, P^m_n] \} \tag{2}$$

here $t[\ ,\ ]$ is the tangent (gradient) operator. The boundary conditions on points P^m_{n+1} are free.

The assembly of curves $<D^1_n, \ldots, D^4_n; C_n, C_{n+1}>$ is the obtained NURBS surface. This procedure is continuously operating from the first slice to the last one until all the object will be covered by NURBS surfaces. The procedure in general is quite simple if the number of curves is the same at each slice, however for the complex geometry there is a number of common cases must be considered specifically. Because all curves in case of MRI-generated object is closed contours, specific algorithms cases and exclusions must be applied, which are explained in following paragraphs

2.3.1. *One-to-One Transition with branching (OOTB).* This case operates with two closed contours, one on each slice. In some cases the minimal distance problem from point to the curve has more than one solution (Figure 5). In this situation both solutions are preserved and next slice will contain more points. New surface is created with three containing curves (red).

2.3.2. *Two-to-One Transition (TOT).* This case appears when n-th slice contains more contours than (n+1)-th. In Figure 6 an example of this situation is shown. First, the D^1_n is evaluated as the shortest straight line between two contours of slice n:

$$D^1_n = D^1_n\{ P^{1,6}_n; P^{1,6}_{n_2} \mid \|P^{1,6}_n, P^{1,6}_{n_2}\| = \min\|C^1_n, C^2_n\| \} \tag{3}$$

2.3.3. One-to-Many Transition (OMT). In this situation one of the OOTB, TOT, or MOT procedures is inversed and applied. Note that it is only the points and straight lines are found inversely. For the normal regions after the transition region evaluation the normal procedure should follow.

2.3.4. *First and last slices.* For the first and last slices the trimmed surface are generated based on contours. First set of NURBS between first and second slice are generated with the minimal curvature BC on both cases. The final set of NURBS surfaces uses the minimal curvature condition only on the final end.

2.3.5. *Other exclusions.* There are lots of other different cases and exclusions less commonly have been met during the procedure, but generally it is the problems of programming, counting points, and algorithm implementing. The entire procedure was implemented using C++ using with internal CAD
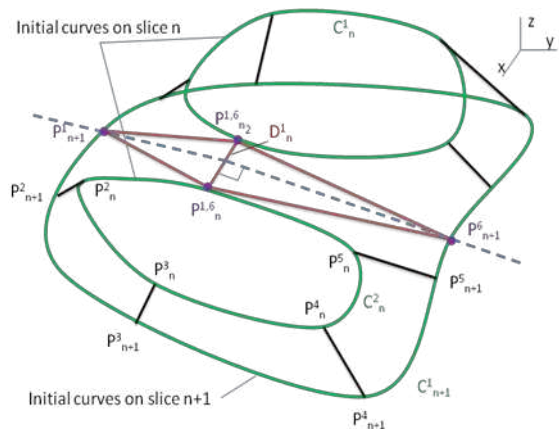
library for standard lofting functions. The result of the procedure implemented for human brain reconstruction could be observed in Figure 8.
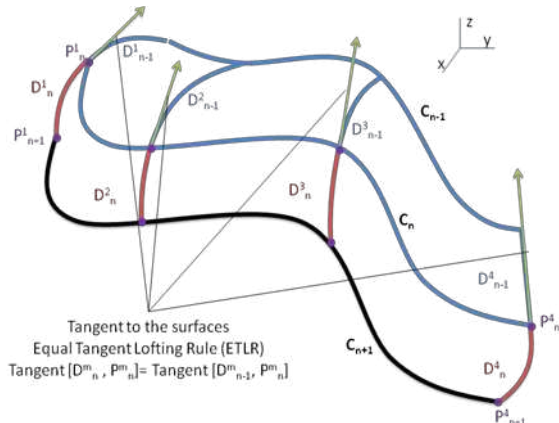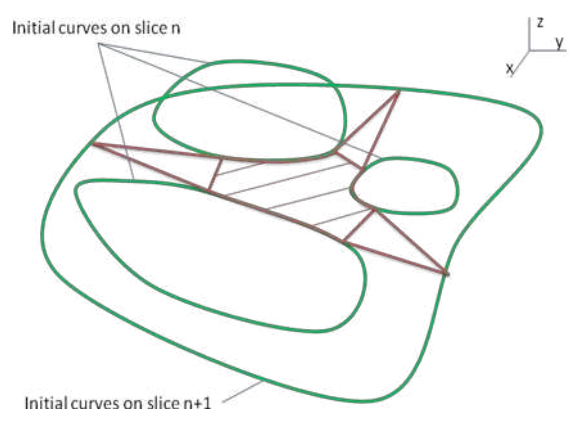

Figure 4. Lofting procedure with 3 slices (see explanations in text).
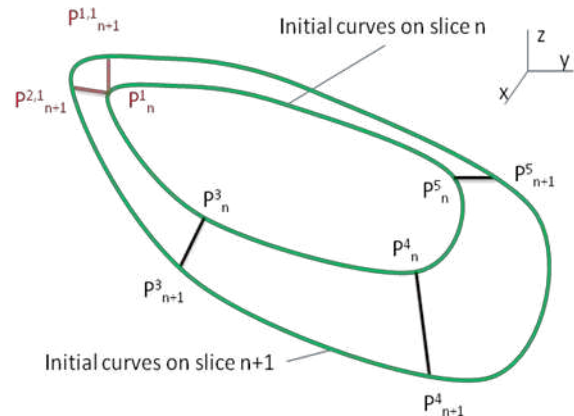
Figure 5. Points branching in One-to-One transition case.

Figure 6. Two-to-One Transition case.


Figure 7. Many-to-One Transition case.

The white matter external boundaries after Lofting Procedure implementation could be seen in Figure 9. Top view represents general overview of NURBS model, and bottom picture is shown in perpendicular to the slice planes projection. The parameters of the full brain model could be observed in Table 1. Obtained model is stored in CAD format and is ready for transferring into any computational environment for simulation.

2.4. *3D geometrical solid model smoothing option.*

Reconstructed model is very accurate in terms of geometry, and according to the presented algorithm it reaches the theoretical limitations of MRI as there is no accuracy loss during the reconstruction process. However, in some cases, for example for testing solution or for any other proposes, where accuracy is not so important, less accurate and lighter model may be required. In those cases the Smoothing Procedure is developed. It is optional, and therefore, the accuracy of obtaining geometry was not tested. This procedure is based on temporary triangularization and NURBS smoothing algorithm, which could be performed using any existing reverse engineering software. The result after smoothing procedure being done is shown in Figure 10.

**Table 1.** Parameters of the solid NURBS model of the human brain

Parameter	Value
Number of slices	150
Total number of NURBS surfaces in white matter boundaries	30 000
Total number of NURBS surfaces in grey matter boundaries	10 000
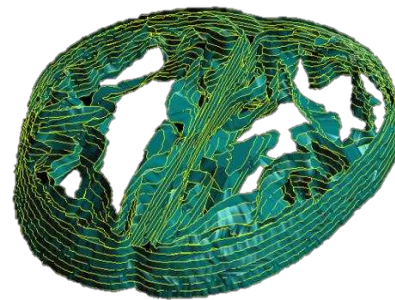
Figure 8. Automatic Lofting Procedure in process. Human brain. grey matter (external) and white matter (internal) NURBS for 7 slices could be observed.
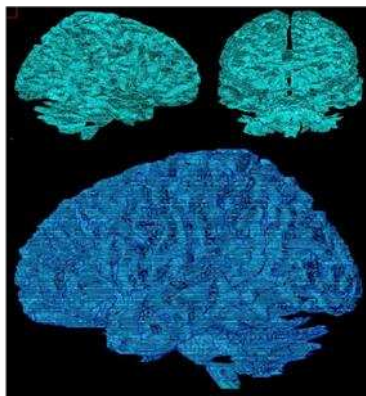
Figure 9. White matter external NURBS surfaces after Lofting Procedure implementation.
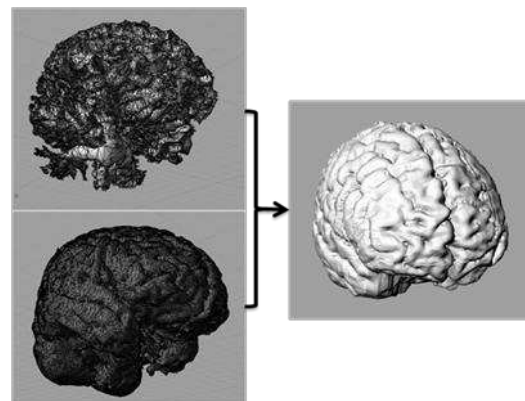
Figure 10. Brain model after smoothing procedure.

3. Accurate material properties reconstruction

Material properties reconstruction is required when starting computer simulations. The accuracy of the material properties has the same importance level as the geometry. Therefore the special reconstruction algorithm was developed to obtain human brain electrical properties, more specifically conductivity of the brain tissue.

Brain tissue, especially white matter has complex fiber structure, and therefore complex anisotropic properties. These properties, however, could be measure with using Diffusion Tensor MRI technique (DTMRI) [8-9]. Diffusion tensor in the entire brain could be obtained and processed into the conductivity tensor by following equation. The underlying assumption is that the same structural features that result in anisotropic mobility of water molecules (detected by DT-MRI) also result in anisotropic conductivity. The quantitative expression for this assumption is that the eigenvectors of the conductivity tensor are the same as those from the water diffusion tensor [10]. Therefore, in projection on the main axis conductivity tensor **C** should be directly proportional to the diffusion tensor **T**:

$$\mathbf{C} = k\mathbf{T}$$

(4)

where k is the scalar coefficient, and could be obtained using mean values of the tensors, which is average conductivity for the grey matter, and it is known by direct measurement. In order to obtain Diffusion tensor for the existing geometry model, DTMRI scan for the same subject was taken as initial income data. All property-related algorithms were implemented in FE level of study.

3.1. Diffusion tensor estimation

It is possible with DTMRI to operate directly with voxels, on which entire space is meshed. For each DTMRI voxel the diffusion tensor estimation has been done. In Figure 11 the resulting diffusion tensor is shown for one layer of voxels. Each tensor value is represented as a rectangular coloured block. Each side length of the block is scaled according to corresponding eigenvalue of diffusion tensor and oriented parallel to corresponding eigenvector. Color shows the principal tensor axis orientation with red indicating mediolateral, green anteroposterior and blue superoinferior direction.

3.2. Conductivity tensor estimation

Diffusion tensor then was converted into the conductivity tensor with coefficient k evaluation. The example of resulting conductivity tensor voxels could be seen in Figure 12. Again the sizes of the box side and its orientation represent corresponding eigenvalues and eigenvectors, and color shows appropriate orientation of the principal tensor axis.
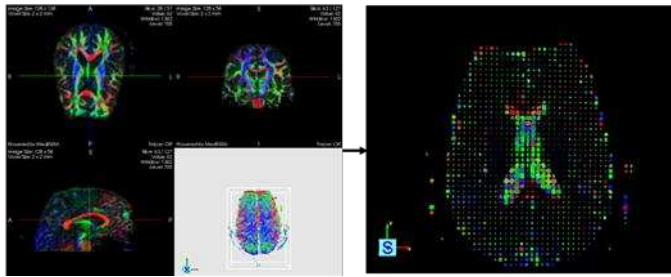
Figure 11. Diffusion tensor estimation (see text for details).
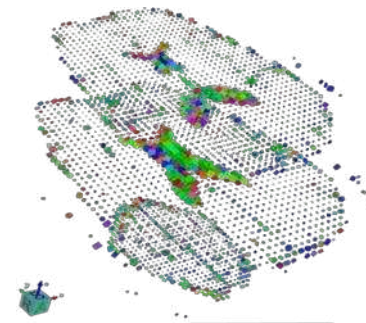
Figure 12. Conductivity tensor for human brain tissue. Three voxel layers are presented.

4. Some results of FE simulations

In order to test both geometrical and material properties reconstruction routines the testing showcase was solved. This case is developed to show the anisotropic conductivity influence on the solution of bioelectromagnetic problems. The computational set-up with mesh could be seen in Figure 13. The problem is formulated as static electrical conduction problem with potential difference applied. In case of isotropic homogeneous conductivity the solution for the current path is straight line.

Because of parametric representation mesh convergence analysis were made before the solution which on author's knowledge never occurred before in computational bioelectromagnetic problem with human brain models. In Figure 14 the resulting current paths are shown after simulation were performed. It is clearly seen that the current takes complex shape according to the anisotropy of conductivity tensor. Resulting current path is shown in three projections on and isometric view inside the brain. Color shows the current density of particular segment of current path (from blue to red).

5. Conclusions

Automatic routine for the accurate 3D model reconstruction of biological objects have been developed and was discussed in this paper. Geometrical 3D model reconstruction procedure requires only initial parameters being set up, such as filtering options, MRI data and parameters, and geometrical accuracy criteria, which sometimes matches with theoretical resolution of MRI method. Procedure could be implemented being fully automatic. Existing implementation allows full geometrical 3D CAD model to be obtained in approximately two days. However, it is possible to further improve this routine and work is continued in order to achieve required speed of reconstruction. According to the mathematical methods underlying developed algorithms geometrical

reconstruction routine could be used with any imaging modality and has ability for reconstructing any biological object.

Material properties reconstruction routine for brain tissue anisotropic conductivity was also developed and tested. Brain model, obtained with highlighted techniques is known to be the most accurate in terms of both geometrical and material properties. Obtained human brain model successfully transferred into the finite element software and testing solution is successfully performed. It is essential that the model, reconstructed with developed algorithms has standard CAD format and also could be used in any simulation software which supports this very common parametric format.

Described routines and tools, once optimized in terms of time of reconstruction, could be integrated with existing imaging hardware in order to obtain 3D models of the internal biological structures for particular subjects.
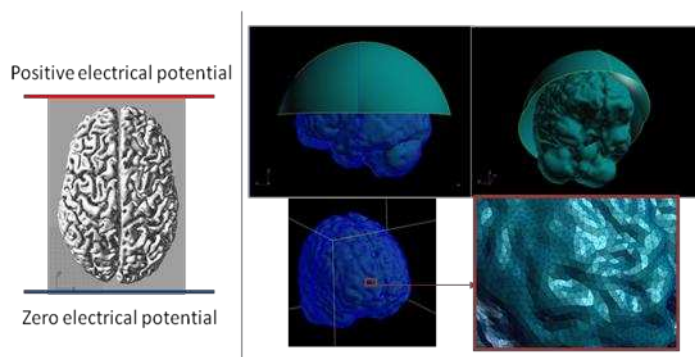
Figure 13. Computational set-up for FE analysis. The problem description (left), and FE mesh observation (right).
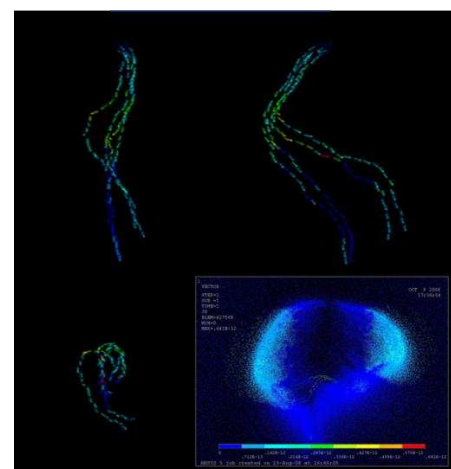
Figure 14. Results of the test problem. Current paths visualization.

6. References

[1]   Landini L, Positano V and Santarelli M F 2005 *Advanced image processing in magnetic resonance imaging* (Boca Raton, FL: CRC/Taylor & Francis)

[2]   CIT *Mipav software* Available: http://mipav.cit.nih.gov/index.php

[3]   Green J A 1994 *Optimal edge detection and digital picture processing* (Wichita, Kan.: Greenwood Research)

[4]   Russ J C 2007 *The image processing handbook* (Boca Raton: CRC/Taylor and Francis)

[5]   Vaseghi S V 2008 *Advanced digital signal processing and noise reduction* (New York: J. Wiley & Sons)

[6]   Berg M d 2008 *Computational geometry : Algorithms and applications* (Berlin: Springer)

[7]   Boissonnat J D and Teillaud M 2007 *Effective computational geometry for curves and surfaces* (New York ; Berlin: Springer)

[8]   Jung Y, Samsonov A A, Block W F, Lazar M, Lu A, Liu J and Alexander A L 2009 3d diffusion tensor mri with isotropic resolution using a steady-state radial acquisition *J Magn Reson Imaging* **29** 1175-84

[9]   Yeo T V, Fillard P, Pennec X, Golland P, Ayache N, and Clatz O 2008 Dti registration with exact finite-strain differential *Proceedings of the IEEE International Symposium on Biomedical Imaging: From Nano to Macro (ISBI'08)*

[10]   Basser P J, Mattiello J and LeBihan D 1994 Mr diffusion tensor spectroscopy and imaging *Biophys J* **66** 259-67